CrossMark

A new equation for activity calculation in pulse irradiation: derivation, simulation, and experimental validation

Zaijing Sun[1]

Abstract To calculate the radioactivity of product nuclides generated in pulse irradiation, it is generally assumed that the irradiation is approximately continuous in the entire irradiation period (t_i) and the flux of the incoming irradiation particle can be obtained by averaging their intensity in each pulse period (T). However, this approximation fails to acknowledge the fact that the product nuclides are not created in each pulse period (T) evenly: They are only produced in a very short pulse width (t_p) and then decay in a relatively long rest time ($t_r = T - t_p$). Given by the enormous number of pulses, the sum of these decays may not be negligible. To make the activity calculation in accordance with the real situation in pulse irradiation, we scrutinize the details of irradiation and decay processes in each pulse, apply the geometric series to obtain the activity superimposition of millions of pulses, and derive a novel activity equation particularly suitable for pulse irradiation. The experimental results, numerical simulations, and activity measurements from photon activation driven by a pulsed electron LINAC have confirmed the validity of this new equation. The comparison between the new and traditional equations indicates that their discrepancy could be significant under certain conditions. The limitations of the new activity equation for pulse irradiation are discussed as well.

Keywords Activity equation · Geometric series · Continuous irradiation · Pulse irradiation

1 Introduction

Radioactivity calculation is a primary concern in nuclear activation analysis, medical isotope production, health physics, and other fields in nuclear and radiological sciences. Historically, the activity may be generated from sources which are capable of continuous radiation, such as nuclear reactors and radioisotope resources. The number of product nuclides $N(t_i)$ at the end of irradiation time t_i follows the equation

$$N(t_i) = \frac{R}{\lambda} \cdot \left(1 - e^{-\lambda t_i}\right) = \frac{N_0 \varphi \sigma}{\lambda} \cdot \left(1 - e^{-\lambda t_i}\right), \quad (1)$$

where R is the reaction rate of selected nuclear reaction, N_0 is the original number of target nuclides, λ is the decay constant of product nuclides, φ is the particle flux of the irradiation particle (e.g., high-energy photon or thermal neutron), and σ is the cross section of corresponding nuclear reaction. The product $\varphi \sigma$, or reaction rate density, is usually an integral over the energy of the incoming particle from threshold energy in which the reaction occurs to the maximum energy ($\varphi \sigma = \int_{E_{threshold}}^{E_{max}} \varphi(E)\sigma(E)\mathrm{d}E$). The burn-up of target nuclides is usually very small and could be ignored in most situations. The total number of radionuclides N follows the curve in Fig. 1a, which reaches its peak $N(t_i)$ at the end of irradiation and then decays according to the exponential law. The activity at this

✉ Zaijing Sun
zsun@scsu.edu

[1] Nuclear Engineering Program, South Carolina State University, 300 College Street NE, Orangeburg, SC 29117, USA

Fig. 1 **a** Number of the product nuclides in continuous irradiation assumption; **b** number of the product nuclides in pulsed irradiation (highly exaggerated)

(a)   **(b)**
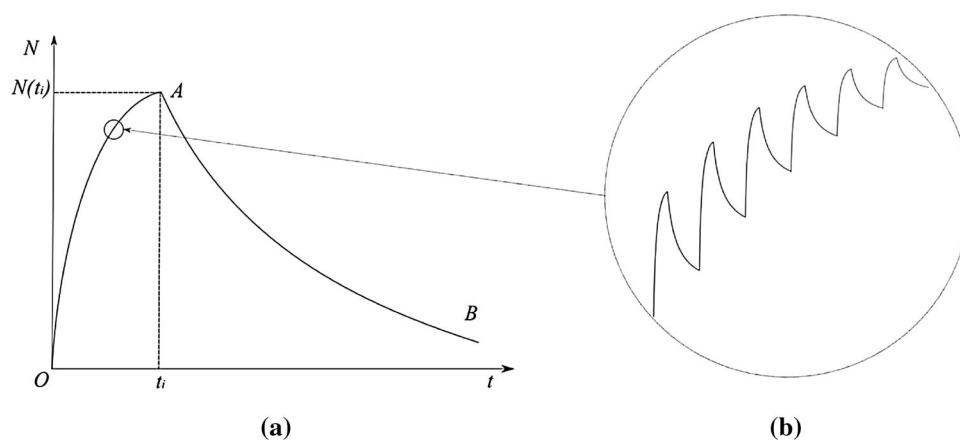
moment always equals the peak number of product nuclides times the decay constant

$$A(t_i) \equiv \lambda N(t_i) = R\left(1 - e^{-\lambda t_i}\right) = N_0 \varphi \sigma \left(1 - e^{-\lambda t_i}\right). \quad (2)$$

Nowadays, due to the development of accelerator technology, more and more radioisotopes are produced by pulse irradiation [1]. Traditionally, to calculate the activity from pulse irradiation, scientists usually expand the usage of continuous irradiation Eqs. (1) and (2) into applications of pulse irradiation without too much consideration of details in pulses. Instead of peak flux in the pulse width, they use average particle flux during the whole irradiation period to calculate the final radioactivity [2–5]. This practice does make sense at the first thought: The repetition rate of pulses is usually relatively high, the irradiation can be regarded as continuous from the point of whole irradiation period, and the half-life of the product nuclides of interest is usually long even comparable to the whole irradiation time.

However, the continuous assumption is questionable when more details of each pulse are revealed. Figure 1a shows the number of product nuclides for a continuous irradiation source such as a nuclear reactor. The product nuclides start to grow from zero when the irradiation starts ($O \rightarrow A$), reach the peak point (maybe close to saturation) at point A when the irradiation stops at t_i, and then decay exponentially after irradiation ($A \rightarrow B$). If the irradiation is driven by a pulsed irradiation source (e.g., LINAC), the curve of activation period (OA) is not as smooth as in Fig. 1a. Imagining we use a magnified glass to see the details of OA, it is more like Fig. 1b. The zigzag shape (or a series of superimposed bumps) shows growth and decay within the pulses. Even though the overall trend of number of product nuclides is growing, there are drops in pulses, which come from the decay in the rest (or down) time among pulses. Some product radioisotopes have very short half-lives, and the total irradiation period is relatively long. With millions of pulses, the total sum of rest time is not

negligible. For instance, in 10-h irradiation of a typical L-band electron LINAC which has pulse width in microsecond (see Fig. 2a), the total uptime (addition of millions of pulse widths) is only in the scale of minutes, and the remaining time (or total rest time) is about 9.9 h simply for the accelerator to prepare for the next pulse. Given the enormous number of pulses, it looks suspicious to adapt continuous assumption and ignore the decay process during pulses.

What does the activity equation look like if we adapt the pulsed irradiation model instead? Does the pulse activation model impact significantly on the results of the final activity of radioisotopes? Which physical parameter(s) in pulse irradiation will significantly affect the final activity of product nuclides? To answer these questions and make the activity calculation more accurate, one needs to establish a new pulse irradiation model in accordance with the real experimental situation in pulse irradiation.

2 Theoretical: mathematical derivations of general activity equation in pulse irradiation

In real situation of irradiation, the pulse profile is very complicated (see Fig. 2a). It may be the overlap of several sinusoidal waves. In the following discussion, a simplified pulse profile as a rectangular wave in Fig. 2b is introduced: I_p is the pulse current, $\bar{I}$ is the average current, t_p is pulse width, t_r is the rest time in each pulse, and $T\left(= t_p + t_r\right)$ is the pulse period, which is the reciprocal of the repetition rate (or frequency) f.

2.1 Derivation 1: superimposition of activities from each pulse at the end of irradiation

Initially, it looks like a tedious work to calculate the total number of product nuclides after an irradiation period t_i due to millions of pulses. However, this can be solved by

Fig. 2 (Color online) **a** An oscilloscope shows the pulse profile for the LINAC at the low-energy accelerator facility (LEAF) at Argonne National Laboratory; **b** rectangular wave model for pulse irradiation

(a)

(b)
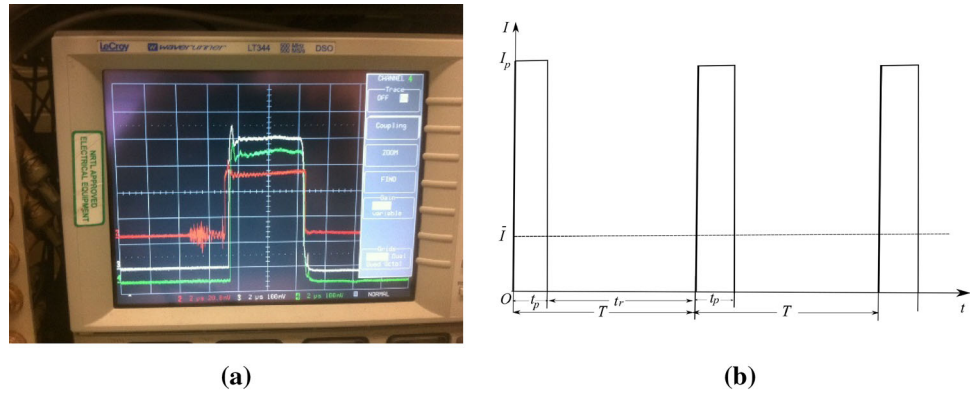
the superimposition of millions of pulses (bumps) using convergent geometry series. The final number of product nuclides is the superimposition of a series of bumps which are illustrated in Fig. 2b or in Fig. 3. Each bump corresponds to one pulse irradiation. The total number of product nuclides at the moment t_i is the sum of all the residual product nuclides at the moment t_i produced by each pulse. Each pulse creates radioisotopes independently, and they are not in contact with each other.

For the first pulse, it created N_p product nuclides in pulse width time t_p. At the moment of t_i, product nuclides generated from the first pulse have decayed with a time period of $t_i - t_p$. Thus, according to the decay law, one gets the number of residual product nuclides produced by the first pulse at the moment of t_i as

$$N_1 = N_p e^{-\lambda\left(t_i - t_p\right)} = N_p e^{\lambda t_p} e^{-\lambda t_i}. \tag{3}$$

For the second pulse, it created N_p product nuclides in pulse width time t_p as well. (The burn-up of target nuclide is ignored.) At the moment of t_i, the decay time for the

second pulse is $t_i - t_p - T$. The number of residual product nuclides produced in the second pulse is

$$N_2 = N_p e^{-\lambda\left(t_i - t_p - T\right)} = N_p e^{\lambda t_p} e^{-\lambda t_i} e^{\lambda T}. \tag{4}$$

For the third pulse, at the moment of t_i, the decay time is $t_i - t_p - 2T$ and

$$N_3(t_i) = N_p e^{-\lambda\left(t_i - t_p - 2T\right)} = N_p e^{\lambda t_p} e^{-\lambda t_i} e^{2\lambda T}. \tag{5}$$
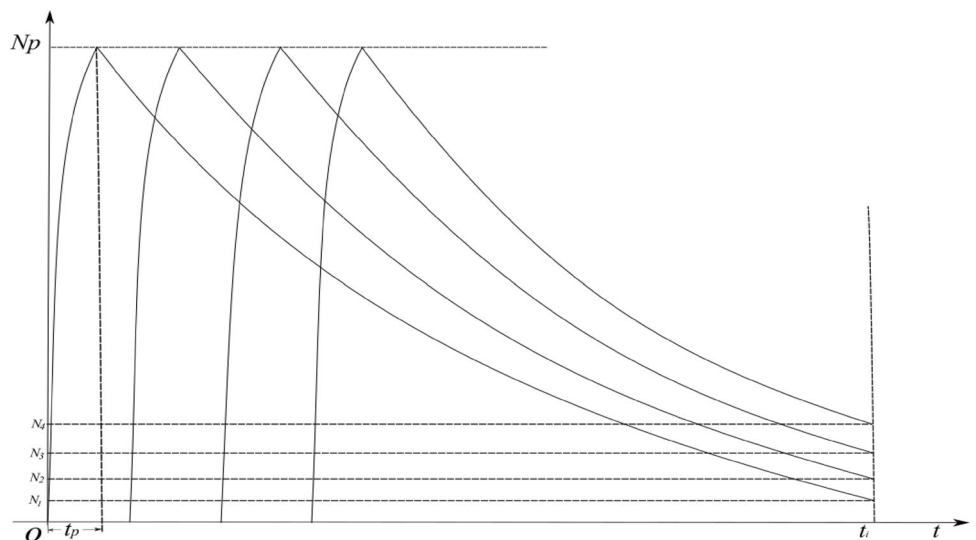
Accordingly, for the last pulse m before the end of irradiation, the number of residual product nuclides is

$$N_m(t_i) = N_p e^{-\lambda\left(t_i - t_p - (m-1)T\right)} = N_p e^{\lambda t_p} e^{-\lambda t_i} e^{(m-1)\lambda T}. \tag{6}$$

The total of residual product nuclides at the end of irradiation is

$$
\begin{aligned}
N(t_i) &= N_1 + N_2 + N_3 + \cdots + N_m \\
&= N_p e^{\lambda t_p} e^{-\lambda t_i} \left(1 + e^{\lambda T} + e^{2\lambda T} + \cdots + e^{(m-1)\lambda T}\right) \\
&= N_p e^{\lambda t_p} e^{-\lambda t_i} \sum_{j=1}^{m} e^{(j-1)\lambda T}.
\end{aligned}
\tag{7}
$$

Fig. 3 Superimposition of pulses (bumps) using geometry series

Let

$$s = \sum_{j=1}^{m} e^{(j-1)\lambda T} = 1 + e^{\lambda T} + e^{2\lambda T} + \cdots + e^{(m-1)\lambda T}. \quad (8)$$

To get the limit of the convergent geometric series above, we multiply $e^{\lambda T}$ on both sides

$$\begin{aligned} e^{\lambda T} s &= e^{\lambda T} + e^{2\lambda T} + \cdots + e^{(m-1)\lambda T} + e^{m\lambda T} \\ &= 1 + e^{\lambda T} + e^{2\lambda T} + \cdots \\ &\quad + e^{(m-1)\lambda T} + e^{m\lambda T} - 1 \\ &= s + e^{m\lambda T} - 1. \end{aligned} \quad (9)$$

By rearranging (9), one gets

$$s = \frac{e^{m\lambda T} - 1}{e^{\lambda T} - 1}. \quad (10)$$

The relation between m and t_i is

$$m = \mathrm{int}\left(\frac{t_i}{T}\right). \quad (11)$$

By inserting Eq. (11) into Eq. (10), one obtains

$$s = \frac{e^{\mathrm{int}\left(\frac{t_i}{T}\right)\lambda T} - 1}{e^{\lambda T} - 1} \approx \frac{e^{\frac{t_i}{T} \times \lambda T} - 1}{e^{\lambda T} - 1} = \frac{e^{\lambda t_i} - 1}{e^{\lambda T} - 1}. \quad (12)$$

Combining Eq. (12) with Eq. (7) yields

$$N(t_i) = \frac{N_p e^{\lambda t_p} e^{-\lambda t_i}(e^{\lambda t_i} - 1)}{e^{\lambda T} - 1} = \frac{N_p e^{\lambda t_p}(1 - e^{-\lambda t_i})}{e^{\lambda T} - 1}. \quad (13)$$

In the pulse width t_p, the irradiation is continuous and $\varphi = \varphi_p$. Combining Eq. (13) with Eq. (1), one obtains:

$$N(t_i) = \frac{N_0 \varphi_p \sigma e^{\lambda t_p}\left(1 - e^{-\lambda t_p}\right)\left(1 - e^{-\lambda t_i}\right)}{\lambda(e^{\lambda T} - 1)}. \quad (14)$$

2.2 Derivation 2: addition of nuclides generated by each pulse

Derivation 1 is based on the superimposition of residual radioactive nuclides produced by each pulse at the end of moment t_i. To some extent, it is slightly counterintuitive. The logical way is to follow the time sequences: The growth of activity should be calculated one pulse after another pulse from the start to the end of irradiation. In this section, we will follow this logic and prove that two derivations reach the same result. For the convenience of discussion, we assume that the burn-up of target nuclides is negligible and the number of product nuclides suddenly increased N_p at the end of each t_p (see the sketch in Fig. 4).

For the first pulse, OA is a continuous irradiation, at point O

$$N_{1,1} = 0. \quad (15)$$

At point A, the number of product nuclides is

$$N_{1,2} = N_p. \quad (16)$$

For the second pulse, it starts at point B

$$N_{2,1} = N_{1,2}e^{-\lambda(T-t_p)} = N_p e^{-\lambda(T-t_p)} = N_p e^{\lambda t_p}e^{-\lambda T}. \quad (17)$$

At point C, compared with the point X where B decays after a period of t_p, the number of nuclides increases N_p, and thus

$$\begin{aligned} N_{2,2} &= N_{2,1d} + N_p = N_{2,1}e^{-\lambda t_p} + N_p = N_p e^{\lambda t_p}e^{-\lambda T}e^{\lambda t_p} + N_p \\ &= N_p\left(e^{-\lambda T} + 1\right). \end{aligned} \quad (18)$$

Accordingly, for the third pulse (DE)

$$\begin{aligned} N_{3,1} &= N_{2,2}e^{-\lambda(T-t_p)} = N_p\left(e^{-\lambda T} + 1\right)e^{-\lambda(T-t_p)} \\ &= N_p e^{\lambda t_p}\left(e^{-2\lambda T} + e^{-\lambda T}\right), \end{aligned} \quad (19)$$

$$\begin{aligned} N_{3,2} &= N_{3,1d} + N_p = N_{3,1}e^{-\lambda t_p} + N_p \\ &= N_p\left(e^{-2\lambda T} + e^{-\lambda T} + 1\right). \end{aligned} \quad (20)$$

For the last pulse m before the end of irradiation, we have

$$N_{m+1,1} = N_p e^{\lambda t_p}\left(e^{-m\lambda T} + \cdots + e^{-\lambda T}\right) = N_p e^{\lambda t_p}\sum_{j=1}^{m} e^{-j\lambda T}. \quad (21)$$

Similar to derivation 1, we can get the limit of the convergent geometric series as

$$\sum_{j=1}^{m} e^{-j\lambda T} = \frac{1 - e^{-\lambda t_i}}{e^{\lambda T} - 1}. \quad (22)$$

By combining Eqs. (22), (21), and (1),

$$N_{m+1,1} = \frac{N_0 \varphi_p \sigma e^{\lambda t_p}\left(1 - e^{-\lambda t_p}\right)\left(1 - e^{-\lambda t_i}\right)}{\lambda(e^{\lambda T} - 1)}, \quad (23)$$

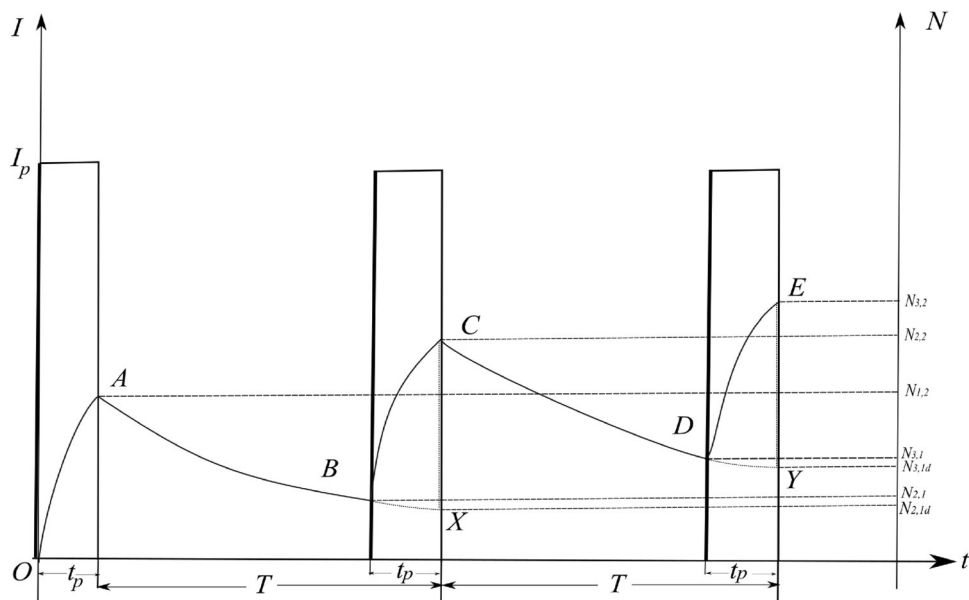which is exactly the same as the result of Eq. (14).

2.3 General activity equation for pulse irradiation

Since $T = t_p + t_r$, Eq. (14) or (23) can be modified as

$$\begin{aligned} N(t_i) &= \frac{N_0 \varphi_p \sigma e^{\lambda t_p}\left(1 - e^{-\lambda t_p}\right)\left(1 - e^{-\lambda t_i}\right)}{\lambda(e^{\lambda T} - 1)} \\ &= \frac{N_0 \varphi_p \sigma\left(1 - e^{-\lambda t_p}\right)\left(1 - e^{-\lambda t_i}\right)}{\lambda(1 - e^{-\lambda T})} \cdot \frac{e^{\lambda t_p}}{e^{\lambda T}} \\ &= \frac{N_0 \varphi_p \sigma\left(1 - e^{-\lambda t_p}\right)\left(1 - e^{-\lambda t_i}\right)}{\lambda(1 - e^{-\lambda T})} \cdot e^{-\lambda t_r} \end{aligned} \quad (24)$$

And the final activity at the end of pulse is

Fig. 4 Addition of activity generated by each pulse

$$A(t_i) = \frac{N_0 \varphi_p \sigma e^{\lambda t_p}\left(1 - e^{-\lambda t_p}\right)\left(1 - e^{-\lambda t_i}\right)}{e^{\lambda T} - 1}$$
$$= \frac{N_0 \varphi_p \sigma (1 - e^{-\lambda t_p})\left(1 - e^{-\lambda t_i}\right)}{(1 - e^{-\lambda T})} \cdot e^{-\lambda t_r}. \tag{25}$$

If one considers the activity right at the end of last pulse width t_p, the decay factor $e^{-\lambda t_r}$ vanishes. This term can be seen as a factor generated by the rest time in the last pulse. Thus, at the end of last pulse width, the total number of product nuclides N_{total} and the corresponding activity A_{total} are

$$N_{\text{total}} = \frac{N_0 \varphi_p \sigma \left(1 - e^{-\lambda t_p}\right)(1 - e^{-\lambda t_i})}{\lambda (1 - e^{-\lambda T})}, \tag{26}$$

$$A_{\text{total}} = \frac{N_0 \varphi_p \sigma \left(1 - e^{-\lambda t_p}\right)\left(1 - e^{-\lambda t_i}\right)}{1 - e^{-\lambda T}}. \tag{27}$$

Equation (27) is the general activity equation for pulse irradiation. If $t_p = T$, or in other words, the irradiation is continuous, then Eq. (27) changes its form back to Eq. (2), which is the general activity equation for continuous irradiation.

From Eq. (27), one can notice that the activity of product nuclides is not only related to λ, N_0, φ, and σ, but also determined by three time parameters: t_p, t_i, and T. The final activity in pulse irradiation is proportional to the saturation factor $1 - e^{-\lambda t_p}$ of irradiation in the pulse width t_p and the saturation factor $1 - e^{-\lambda t_i}$ of irradiation in the whole irrational period t_i. In addition, it is also inversely proportional to the saturation factor $1 - e^{-\lambda T}$ of irradiation in the pulse period T.

3 Experimental: photon activation with pulsed electron LINAC

3.1 Photon activation experiments

To validate the new activity equation in pulse irradiation, photon activation experiments were conducted by the 44-MeV short-pulsed LINAC at the Idaho Accelerator Center. Figure 5a is the sketch of the experimental setup, which includes electron gun, the electron-—photon converter, and the irradiation sample. Electrons were initially created by hot cathode and then accelerated by a series of alternating RF electric fields in the acceleration cells. Optimized energy around 30 MeV was applied, and the total output power was around 2 kW. The pulse width is 2.3 μs, the repetition rate is 120 Hz, and the peak current is about 240 mA. The electron beam is focused by magnetic fields to a radius of about 3 mm.

After the tungsten converter of 3 mm thickness, the electron beam is completely converted into a bremsstrahlung photon beam. The converter was cooled with forced air continuously to avoid the risk of melting down. The photon flux produced directly after the converter at 30 MeV and 2 kW is approximately 1.1×10^{12} photons/s/cm^2/kW. An aluminum hardener of 7.62 cm was positioned after tungsten block to absorb the residual electrons, and it ensured that the photon beam behind the hardener was predominantly made of high-energy photons. A well-known certified reference material, standard reference material 1648a (urban particulate matter) from NIST, was served as irradiation target [6] and wrapped with aluminum foil into a 1 cm × 1 cm × 1 mm square shape. Target was positioned downstream behind the hardener along the beam
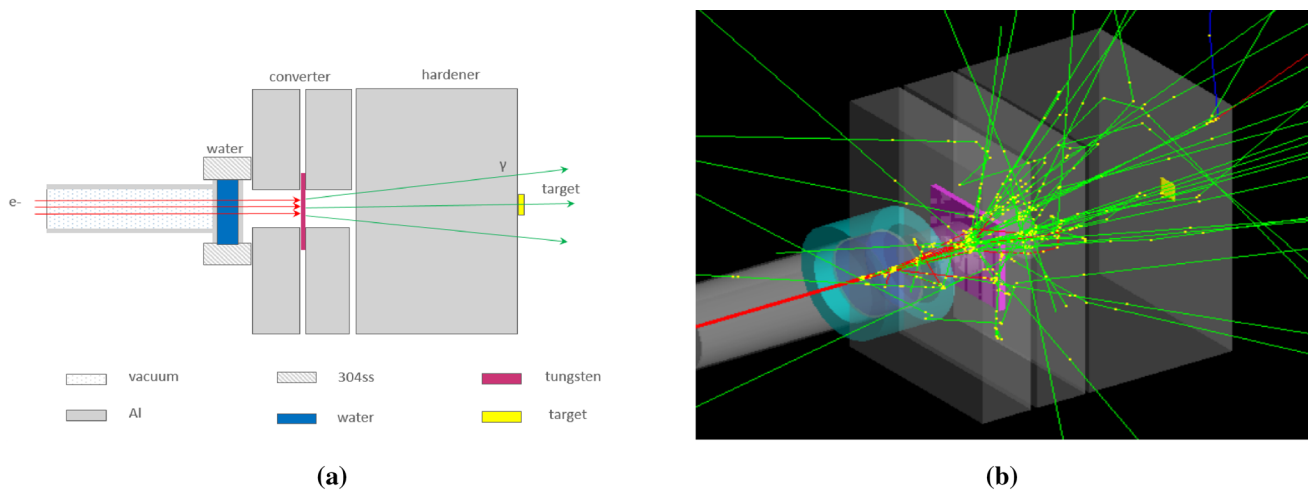
(a)

(b)

Fig. 5 (Color online) **a** Experimental setup of photon activation driven by a pulsed electron LINAC; **b** GEANT4 simulation of photon shower (view point $\theta = 45°$, $\phi = 135°$)

axis to generate activities for measurements. The total irradiation was lasted for 7 h.

3.2 Gamma ray measurements and spectrum analysis

After photon activation, the target was cooled down in the accelerator hall for 24 h to meet the requirement of radiation safety for transferring to the spectroscopy room. Spectra collection was finished by a P-type coaxial detector with 48% efficiency and a resolution less than 1.5 keV. After one week, spectra of long-lived isotopes were collected by the same HPGe detector again. Samples were measured in two positions: J and A. Position J is 10 cm away from the detector head with an intrinsic peak efficiency of 0.00258@393.529 keV for short-lived isotope measurements. Position A is right against the detector with an intrinsic peak efficiency of 0.0625@393.529 keV for long-lived isotope measurements. Figure 6a indicates a

typical gamma spectrum collected by MCDWIN program with some characteristic energy lines and their corresponding radioisotopes [7]. After spectra acquisition, all the gamma spectra files in mp format were the input to Gamma-W software for automatic peak analysis (Fig. 6b) [8].

4 Computational: GEANT4 and MATLAB simulations

4.1 Photon flux simulation with GEANT4

To get the photon flux φ in the sample, Monte Carlo simulations were performed with GEANT4 toolkit 4.10.3 installed on an HP ProDesk 600 G1SFF workstation running a 64 bits Ubuntu 16.04.1 LTS operating system [9–11]. The simulations followed the exact geometry shown in Fig. 5a and generated photon shower illustrated
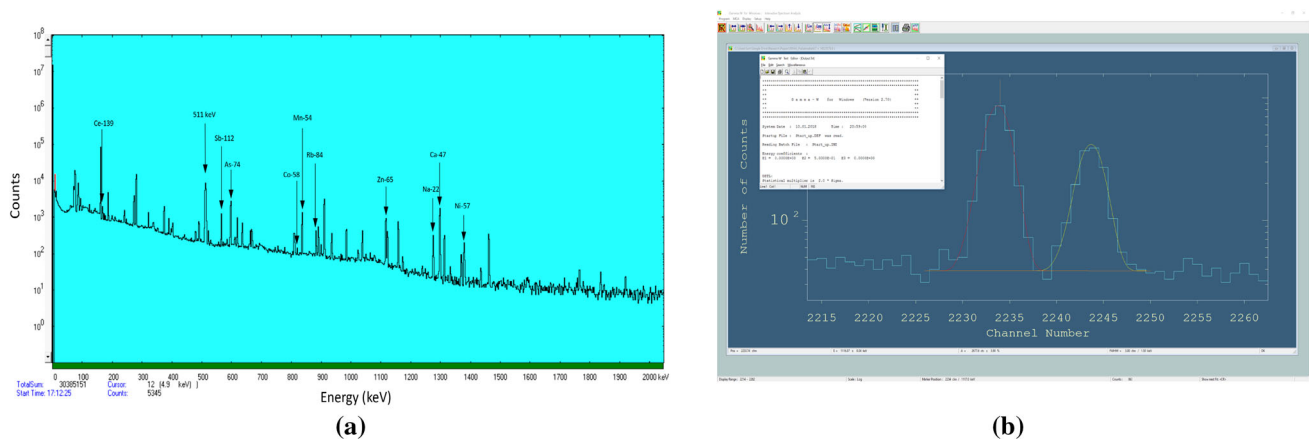

(a)

(b)

Fig. 6 (Color online) **a** A gamma spectrum collected by MCDWIN (*x*-axis energy, *y*-axis counts); **b** peak analysis with Gamma-W program

in Fig. 5b. The relationship between the track color and its corresponding particle is as follows: photon: green, electron: red, positron: blue, neutron: yellow. The magenta block is the tungsten converter, and the yellow flat cuboid right against the hardener simulates the target.

In the physics list file of the photon shower program, all the electromagnetic processes were added, including G4ComptonScattering.hh, G4GammaConversion.hh, G4PhotoElectricEffect.hh, G4eMultipleScattering.hh, G4eIonisation.hh, G4eBremsstrahlung.hh, G4eplusAnnihilation.hh, and G4ionIonisation.hh. To create an electron beam with the measured energy distribution, the default PrimaryGeneratorAction.hh file in the include directory of the program was modified with the class of general particle source (GPS) [12]. A file named "beam.in" stored all the user-defined parameters in energy distribution of the beam. Target material was designed as vacuum on purpose to record all the photons entering the cuboid. The output photon.txt recorded all the photons the target can "see" with the information of their position (x, y, z), energy (E), and momentum (p_x, p_y, p_z).

Figure 7a is the energy distribution of the photons entering the target shown in ROOT framework [13]. One can see that the energy distribution of the photons behaves as a typical bremsstrahlung curve: It starts from zero and ends up with the cutoff energy of the incoming electrons. Figure 7b indicates that the photons are dominantly second-generation particles (parentID = 1). Since the first-generation particles are the incoming electrons (parentID = 0), those photons (parentID = 1) should be created directly by bremsstrahlung process. Some other generations of photons are also created, but their amount is quite limited compared with that of bremsstrahlung photons. These photons might be created by other physics processes, such as pair production, photonuclear reactions.

4.2 Reaction rate density: tabulating photon flux with historical cross section

Six product radioisotopes (^{47}Ca, ^{57}Ni, ^{65}Zn, ^{84}Rb, ^{122}Sb, and ^{139}Ce) and their corresponding photonuclear reactions are selected to validate the activity equation in pulse irradiation. They were chosen based on the following facts: (1) They have clear interference-free energy lines; (2) concentrations of target nuclides are certified; (3) they are products of dominant photonuclear reactions; and (4) their atomic number ranges from low to high in the period table.

Original data of cross section σ is in exchange format (EXFOR), which contains an extensive compilation of experimental nuclear reaction data [14, 15]. Table 1 shows the EXFOR records of the selected photon nuclear reactions. Photon flux φ is the product of electron flux φ_e and photon yield Y. Y is obtained from photon shower simulations by the ratio of the number of photons in a certain energy bin in the target to total incident electrons. Photons in certain energy bins were counted by the histogram function in statistical package R [16]. Cross section data and photon flux in different energy bins were tabulated, and their products are summed up to get the reaction rate density. Table 2 gives an example of the tabulate process for ^{140}Ce(γ,n)^{139}Ce reaction.

In Table 2, E is the energy in MeV, σ is cross section in mb, $\Delta\sigma$ is uncertainty of cross section in mb, "energy bins" is the energy range centered on E, φ_e is number of electrons per second, $Y(E)$ is photon yield in the energy range per square centimeter, $\varphi(E)\sigma(E)$ is the reaction rate density in the energy range in cm^{-2} s^{-1}, $\Delta\varphi(E)\sigma(E)$ is the uncertainty of reaction rate density in the energy range, and $\int_{E_{\mathrm{thres}}}^{E_{\max}} Y(E)_p \sigma(E)_p \mathrm{d}E$ is reaction rate density for the complete energy range.
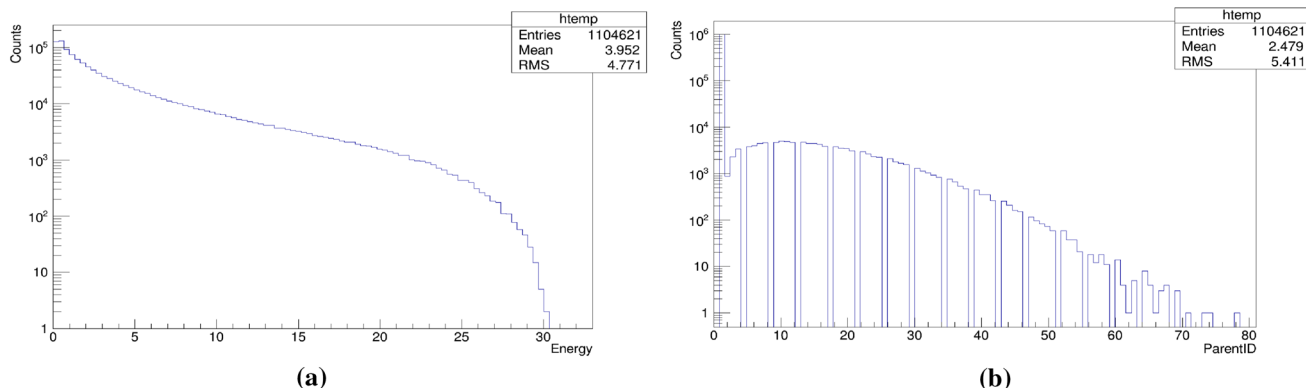

(a)

(b)

Fig. 7 **a** Energy spectra of bremsstrahlung photons simulated by GEANT4 toolkit. **b** The distribution of the generations of the photons in the activation sample

Table 1 Selected photon nuclear reactions and their EXFOR records

Reaction	EXFOR record	Cross section in EXFOR	References
$^{48}Ca(\gamma,n)^{47}Ca$	M0636007	$\sigma(\gamma,n)$	O'Keefe (1987) [14]
$^{58}Ni(\gamma,n)^{57}Ni$	L0034003	$\sigma(\gamma,X)$	Fultz (1974) [14]
$^{66}Zn(\gamma,n)^{65}Zn$	L0164002	$\sigma(\gamma,n)$	Coryachev (1982) [14]
$^{85}Rb(\gamma,n)^{84}Rb$	L0027002	$\sigma(\gamma,X)$	Lepretre (1971) [14]
$^{123}Sb(\gamma,n)^{122}Sb$	L0035033	$\sigma(\gamma,n) + \sigma(\gamma,n+p)$	Lepretre (1974) [14]
$^{140}Ce(\gamma,n)^{139}Ce$	M0367005	$\sigma(\gamma,n)$	Beljaev (1991) [14]

4.3 Numerical simulation with MATLAB

A live script in MATLAB was written to numerically imitate pulse superimposition in the irradiation [17]. All the parameters in scripts are originated from the real experiments conducted in the previous experimental session. The codes of two loops below have been applied with the algorithms in the mathematical session. As we expected, the outputs of numerical simulations from two different algorithms are almost same[1] and they agree with the calculation result from the new equation.

distance from the sample mean to the population mean in units of the standard error. One can see that theoretical activities are in the same order of magnitude as the measured activities. However, the discrepancy in predicted values ranges between 20 and 40%. And all the predicted values are systematically larger than the real experimental values. This is understandable and given by primarily two reasons: (1) The cross section data applied are systemically higher. Because of the lacking cross section data of (g, n) reactions, some cross section data employed are for (γ, n) and $(\gamma, n) + (\gamma, n + p)$ (see Table 1); (2) simulated photon

```
%% Derivation: numerical simulation with loops
% * Derivation 1: Superimposition each pulse at moment t_i
N1 = N_0*phi_p_sigma*(1-exp(-lambda*t_p))*exp(-lambda*(t_i-t_p))/lambda;
for i = (1:m-1) % from 1 to m, run loop, adding exp(-lambda*T) each time
    %disp(i)
    N1 = N1 + N_0*phi_p_sigma*(1-exp(-lambda*t_p))*exp(-lambda*(t_i-t_p-i*T))/lambda;
end
A_p_derivation1 = lambda*N1*exp(-lambda*t_r)  % exp(lambda*t_r) comes from the decay in the last
pulse
% * Derivation 2: Addition of nuclides generated by each pulse one by one
N2=(N_0*phi_p_sigma/lambda)*(1-exp(-lambda*t_p))*exp(-lambda*(T-t_p));
for i = (2:m) % from 2 to m, run loop, adding exp(-lambda*T) each time
   %disp(i)
%N2 = N2 + (N2*exp(-lambda*t_p)+ (N_0*phi_p_sigma/lambda)*(1-exp(-lambda*t_p)))*exp(-lambda*(T-
t_p))
       N2= N2 + (N_0*phi_p_sigma/lambda)*(1-exp(-lambda*t_p))*exp(lambda*t_p)*exp(-lambda*(i*T));
end
A_p_derivation2 = lambda*N2*exp(-lambda*t_r)
%%
```

5 Results and discussion

5.1 Have the experiments confirmed the validity of the general activity equation in pulse irradiation?

Table 3 is the activity comparison between the theoretical predictions from Eq. (27) and the experimental values at the end of irradiation in the photon activation experiments. Experimental values are obtained from measured activities divided by the factor of decay $e^{-\lambda t_d}$. Discrepancy is the difference between experimental values and theoretical predictions in percentage. Z-score is the

flux is usually higher than the real situation. Historical experiments and computer simulations with different Monte Carlo codes have shown that simulated flux is usually higher than the real experimental flux by around 20%, varied by different experimental setups and simulation programs [18]. Besides these two dominating causes, the discrepancy may also be contributed by a combination of several factors, such as beam emittance, uncertainty of beam current, beam loading, beam wandering, energy dissipation in experimental setup, efficiency measurements.

Figure 8a plots the values in Table 3. One can notice that experimental values are consistent with the predicted values despite some discrepancies. Figure 8b shows the statistical correlation between theoretical predictions and actual measurements. Z test results have shown that the predicted values are statistically close to the experimental

---

[1] The slight difference is originated from the inaccuracy of floating-point arithmetic.

Table 2 Reaction rate density and its uncertainty for ^{140}Ce(γ,n)^{139}Ce reaction

E	σ	$\Delta\sigma$	Energy bins	$Y(E)$	$\varphi(E)\sigma(E)$	$\Delta\varphi(E)\sigma(E)$
7.86	0.1	0.86	7.86–7.98	0.0001279	1.279E−32	1.1E−31
7.98	0.08	0.9	7.98–8.1	0.0001313	1.050E−32	1.18E−31
8.1	0.13	0.88	8.1–8.22	0.0001175	1.528E−32	1.03E−31
8.22	0.01	0.88	8.22–8.34	0.0001221	1.221E−33	1.07E−31
8.34	0	0.9	8.34–8.46	0.0001199	0	1.08E−31
…	…	…	…	…	…	…
21.3	55.78	7.14	21.3–21.42	0.0000165	9.2037E−31	1.1781E−31
21.42	54.7	7.27	21.42–21.54	0.000018	9.846E−31	1.3086E−31
21.54	53.75	7.76	21.54–21.66	0.0000191	1.02663E−30	1.48216E−31
21.66	52.89	8.85	21.66–30	0.0000474	2.50699E−30	4.1949E−31
			Sum $\int_{E_{\text{thres}}}^{E_{\text{max}}} \varphi(E)\sigma(E)\mathrm{d}E = 6.619E{-}28 \pm 1.99E{-}29$			

Table 3 Activity comparison between theoretical prediction and experimental measurement

Reaction	Energy line (keV)	Half-life	Experimental activity (Bq)	Theoretical activity (Bq)	Discrepancy (%)	Z-score
^{48}Ca(γ,n)^{47}Ca	1297.09	4d12h51m40s	386 ± 5	488 ± 85	20.90	1.20
^{58}Ni(γ,n)^{57}Ni	1377.63	1d11h36m40s	238 ± 16	316 ± 39	24.68	2.00
^{66}Zn(γ,n)^{65}Zn	1115.55	244d5h6m40s	77 ± 2	104 ± 12	25.96	2.25
^{85}Rb(γ,n)^{84}Rb	881.61	32d18h23m20s	20 ± 1	33 ± 3	39.39	1.33
^{123}Sb(γ,n)^{122}Sb	564.12	2d17h21m40s	172 ± 4	277 ± 28	37.90	3.75

values. The correlation coefficient confirms that they are directly related ($R \approx 0.99289$).[2] Therefore, statistically, we are able to claim that the experiments of photon activation with LINAC have confirmed the validation of the new equation in pulse irradiation.

5.2 Comparison: pulse irradiation versus continuous irradiation

If the new equation was confirmed by the experiments, does it mean the traditional practice with continuous assumption is invalid and the foundation for photon activation analysis was built on sand? Fortunately, the answer to this question is no. The discrepancy in current and traditional equations is negligible in most photon activation cases. As mentioned before, the traditional method to calculate the activity is based on continuous assumption, which means $\varphi_{\text{p}} t_{\text{p}} = \bar{\varphi} T$ and

$$A_{\text{continous}} = N_0 \bar{\varphi} \sigma \left(1 - e^{-\lambda t_{\text{i}}}\right) = N_0 \varphi_{\text{p}} \sigma \left(1 - e^{-\lambda t_{\text{i}}}\right) \cdot \frac{t_{\text{p}}}{T}. \tag{28}$$

Dividing (27) by (28), one gets the ratio ζ between the activities of pulse irradiation and continuous assumption as

$$\zeta = \frac{A_{\text{pulse}}}{A_{\text{continuous}}} = \frac{T}{t_{\text{p}}} \cdot \frac{1 - e^{-\lambda t_{\text{p}}}}{1 - e^{-\lambda T}} = \frac{T}{t_{\text{p}}} \cdot \frac{1 - e^{-\frac{\ln 2}{\tau} \cdot t_{\text{p}}}}{1 - e^{-\frac{\ln 2}{\tau} \cdot T}}. \tag{29}$$

One can notice that ζ value has nothing to do with the total irradiation time t_{i}, but closely related to the ratio of T/t_{p}. Given by the experimental parameters (the pulses are very dense and the half-life of the product nuclides of interest is relatively long compared with the whole irradiation time) in the traditional photon activation, the ζ value is almost equal to 1 without exception. There is no significant change following either the continuous assumption or the current equation of pulse irradiation.[3]

Then, the question is why bother to use the new equation. We prefer to use current equation because: (1) it is a generic equation for pulse irradiation. It clearly distinguishes the pulse uptime and downtime and acknowledges the fact that the accelerator has its duty cycle. Logically and mathematically, the current equation is correct and avoids the unnecessary approximation of continuous irradiation. The discrepancy in the current and traditional equations may not be significant for photon activation, but it may be significant in some other cases, such as medical isotope production, radiation dose calculations, and nuclear physics. (2) In some extreme cases, the discrepancy in these two equations might be quite significant. For

[3] Philosophically speaking, the argument of continuous assumption or pulse irradiation is a new example of ancient Zeno's paradoxes.
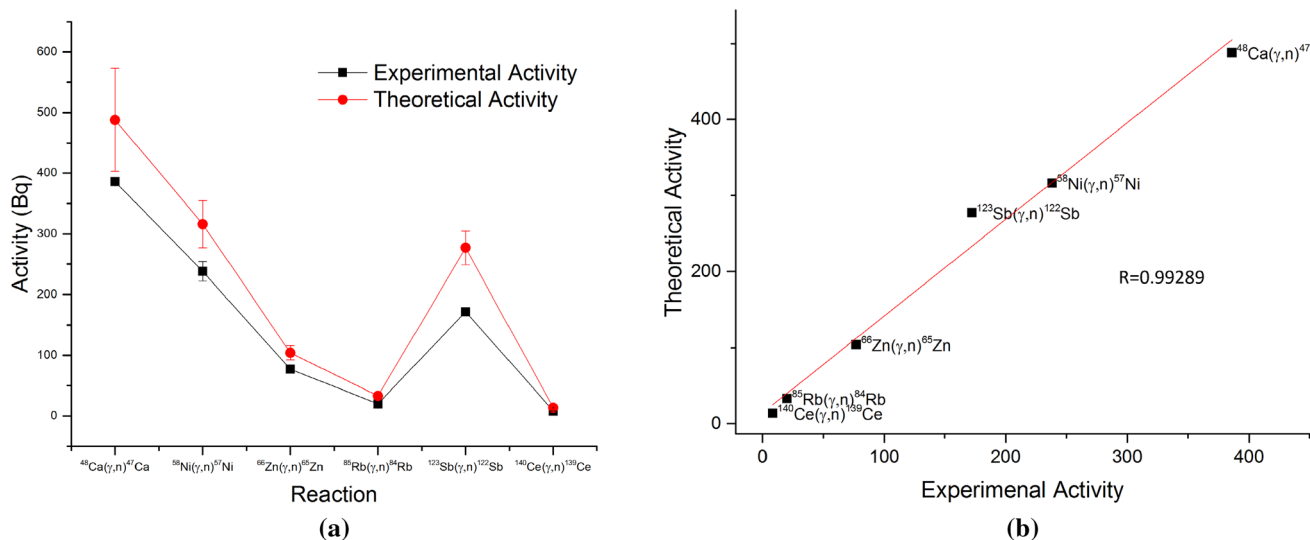
Fig. 8 (Color online) **a** Activity comparison between theoretical prediction and experimental measurement. **b** Z test for activities from theoretical prediction and actual measurements

example, Fig. 9 plots the relationship between τ and ζ in Mathematica within a typical photon pulse irradiation [19]. One can see that ζ changes its values significantly once half-life τ is less than the pulse period T: The shorter the half-life of radionuclide, the larger the ratio ζ, with a maximum value of ζ close to the ratio of T/t_p. When the half-life and pulse period are in the same scale, the ratio is close to 1. Using traditional continuous assumption for those isotopes will not be accurate enough. However, this observation does not impact too much on nuclear activation analysis since what really counts in traditional radioanalytical practice is the ratio of activities, not the absolute activities of the same radioisotope in sample and Refs. [4, 20, 21].

5.3 Further discussions and limitations of the new equation

The relationship between pulse period T and half-life τ of product nuclides not only plays a dominant role in the ratio ζ, but also significantly impacts the final activity of the product nuclides. From the denominator $e^{\lambda T} - 1$ of Eq. (25), one can notice that if $T > \tau$, then the denominator $e^{\lambda T} - 1$ equals $e^{\frac{\ln 2}{\tau} \cdot T} - 1$, which is larger than 1, and the whole fraction is smaller than $\lambda N_0 \phi \sigma e^{\lambda t_p} (1 - e^{-\lambda t_p})(1 - e^{-\lambda t_i})$. On the contrary, if $T < \tau$, the denominator is less than 1, and the result is larger than $N_0 \phi \sigma (1 - e^{-\lambda t_p}) e^{\lambda t_p} (1 - e^{-\lambda t_i})$. Thus, the turning point of activity is decided by the relationship between pulse period T and the half-life τ of the product nuclides. If the pulse period T is significantly shorter than the half-life τ of

product nuclides, one can expect a substantial increase in final activity in pulse irradiation.

Although the current equation is a general equation for pulse irradiation, its usage can be easily broadened to ion beams, reactors operating in pulse mode, and radiation dose calculation, and it has its limitations as well. First of all, it is based on rectangular wave assumption of pulses. In some practical cases, sinusoidal wave assumption might be more accurate. Secondly, it is based on the assumption that the burn-up of target isotope can be negligible in irradiation. If the burn-up cannot be ignored, the current equation of pulse irradiation needs to make some adjustments according to the Bateman's equations [22]. If one considers transient equilibrium, secular equilibrium, and other details in decay kinetics, the final activation equation will be more complicate than the current equation. However, the idea of applying geometry theories to mimic the activity superimposition is still valid.

6 Conclusions

A novel activity equation for pulse irradiation was derived mathematically with the assistance of geometry series, and then, it was confirmed numerically by MATLAB codes and finally validated experimentally by photon activation conducted via a short-pulsed LINAC. The comparison between the new equation (based on pulse irradiation) and the traditional equation (based on an approximation of continuous irradiation) indicates that their discrepancy is negligible in most cases of photon activation, but it could be significant under certain
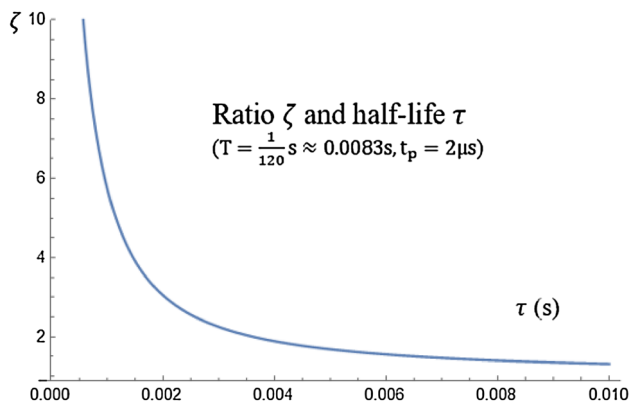
Fig. 9 Activity comparison between pulse assumption and continuous assumption for radioisotopes with very short half-life

conditions. The limitations of the new activity equation are discussed as well.

References

1. V. Starovoitova, C. Segebade, High intensity photon sources for activation analysis. J. Radioanal. Nucl. Chem. (2016). https://doi.org/10.1007/s10967-016-4899-x
2. C. Segebade, A. Berger, Photon activation analysis. Encycl. Anal. Chem. (2008). https://doi.org/10.1002/9780470027318.a6211.pub2
3. S.-H. Liu, X.-B. Jiang, N.-N. Liu, et al., Measurement and calculation of the neutron spectrum and gamma dosimetry of the fast neutron device at Xi'an pulse reactor, in *Nuclear Instruments and Methods in Physics Research Section A, V593(3)*, pp. 361–366, ISSN 0168-9002 (2008). https://doi.org/10.1016/j.nima.2008.05.028
4. Z.J. Sun, D. Wells, C. Segebade et al., A comparison of various procedures in photon activation analysis with the same irradiation setup. Nucl. Instrum. Methods Phys. Res. Sect. B **339**, 53–57 (2014). https://doi.org/10.1016/j.nimb.2014.08.021
5. A. Osman, I. Boztosun, C. Segebade, Multielemental analysis of some soils in Karaman by PAA using a cLINAC. Appl. Radiat. Isot. **122**, 57–62 (2017). https://doi.org/10.1016/j.apradiso.2017.01.011
6. National Institute of Standards and Technology, Certificate of analysis: standard reference material 1648a urban particulate matter, Gaithersburg, MD, USA (2008)
7. FAST ComTech., MCDWIN: MCA emulation and analysis software (2009). https://www.fastcomtec.com/fwww/datashee/mcd/mcdwin.pdf. Accessed 21 Dec 2017
8. W. Westmeier, *Guide to Gamma-W,Sodigam and Alps for Windows, 2009 ed*, 2009th edn. (Dr. Westmeier GmbH, Germany, 2009)
9. S. Agostinelli et al., Geant4—a simulation toolkit. Nuclear Instrum. Methods Phys. Res. Sect. A **506**(3), 250–303 (2003). https://doi.org/10.1016/s0168-9002(03)01368-8
10. J. Allison et al., Geant4 developments and applications. IEEE Trans. Nucl. Sci. **53**(1), 270–278 (2006). https://doi.org/10.1109/TNS.2006.869826
11. Geant4 Collaboration, Geant4 User's Guide for Application Developers (2017). http://geant4.web.cern.ch/geant4/UserDocumentation/UsersGuides/ForApplicationDeveloper/html/index.html. Accessed 21 Dec 2017
12. C. Ferguson, General Purpose Source Particle Module for GEANT4/SPARSET, Physics and Astronomy Department, University of Southampton, Highfield, Southampton, technical note, UoS-GSPM-Tech, Issue 1.1 (2000)
13. CERN, ROOT users guides and manuals (2017). https://root.cern.ch/root/htmldoc/guides/users-guide/ROOTUsersGuide.html. Accessed 21 Dec 2017
14. International Atomic Energy Agency, Handbook on Photonuclear Data for Applications: Cross sections and Spectra, I.A.E.A TECDOC 1178 (2000). http://www-pub.iaea.org/books/IAEABooks/6043/Handbook-on-Photonuclear-Data-for-Applications-Cross-sections-and-Spectra. Accessed 21 Dec 2017
15. B. Pritychenko, V. Zerkin, Experimental nuclear reaction data (EXFOR) (2014), Brookhaven National Laboratory. http://www.nndc.bnl.gov/exfor/exfor.htm. Accessed 21 Dec 2017
16. CRAN, An introduction to R, version 3.4.3 (2017). https://cran.r-project.org/doc/manuals/r-release/R-intro.pdf. Accessed 21 Dec 2017
17. MathWorks, MATLAB: the language of technical computing (2017). https://www.mathworks.com/help/matlab/index.html. Accessed 21 Dec 2017
18. B. Faddegon, Benchmarking of Monte Carlo simulation of Bremsstrahlung from thick targets at radiotherapy energies. Med. Phys. **35**, 4308–4317 (2008). https://doi.org/10.1118/1.2975150
19. Wolfram S. *An Elementary Introduction to the Wolfram Language*, 2nd edn. (2017). http://www.wolfram.com/language/elementary-introduction/2nd-ed/. Accessed 21 Dec 2017
20. R. Greenberg, P. Bode, E. Fernandes, Neutron activation analysis: a primary method of measurement. Spectrochim. Acta Part B **66**, 193–241 (2011). https://doi.org/10.1016/j.sab.2010.12.011
21. C. Segebade, V.N. Starovoitova, T. Borgwardt et al., Principles, methodologies, and applications of photon activation analysis: a review. J. Radioanal. Nucl. Chem. **312**, 443 (2017). https://doi.org/10.1007/s10967-017-5238-6
22. J. Cetnar, General solution of Bateman equations for nuclear transmutations. Ann. Nucl. Energy **33**(7), 640–645 (2006). https://doi.org/10.1016/j.anucene.2006.02.004